Measurements of the Differential Cross Section for the Elastic n–^{3}H and n–^{2}H Scattering at 14.1 MeV by Using an Inertial Confinement Fusion Facility

The development of an accurate description of light-ion reactions is currently of great interest since it would provide valuable insights into low-energy nuclear reactions important to nuclear astrophysics. Radiative capture reactions, for example, occur in red giants at temperatures low enough that the reaction rates are too small to be directly measured in a laboratory. Extrapolation from measurements at higher energies is also suspect without a fundamental theory for computing these reactions. Fusion energy research also requires accurate cross sections for light-ion reactions to constrain models of inertial confinement fusion (ICF) experiments involving deuterium–tritium fuel. For instance, uncertainties in the differential cross section for the elastic n–^{3}H scattering need to be ~5% to reliably infer a fuel areal density (ρR) from the yield ratio between scattered neutrons and primary 14.1-MeV neutrons, called down-scatter ratio (DSR),[1] produced in an ICF implosion. The determination of the ρR from the DSR value is essential for understanding how the fuel is assembled in an implosion and for ultimately guiding the community toward the demonstration of thermonuclear ignition and net energy gain[2] at the National Ignition Facility (NIF).[3]

Since the 1950s, the differential cross section for the elastic n–^{3}H scattering at 14.1 MeV has been subject to both experimental and theoretical studies. Kootsey *et al.*[4] measured the cross section at center-of-mass (CM) angles ranging from 55° to 165°, resulting in data with statistical uncertainties of ~20% and a systematic uncertainty of 11%. Shirato *et al.*[5] and Debertin *et al.*[6] measured the cross section in the CM angular range of 100° to 175° with an uncertainty varying from ~10% to ~70%, and their results are in good agreement with each other, but up to a factor-of-2 smaller than the Kootsey data. Optical-model calculations conducted by DeVries *et al.*[7] and by Sherif and Podmore[8] reproduced the Shirato and Debertin data in this CM angular range. Additionally, Hale *et al.*[9] conducted an *R*-matrix analysis of all experimental data sets, and the result from that analysis forms the basis of the current ENDF/B-VII evaluation[10] of the differential cross section for the elastic n–^{3}H scattering that can be found in nuclear databases. Although efforts have been made to quantify this fundamental cross section, significant discrepancies exist between the different measurements and between measurements and models. However, a theoretical understanding of the n + ^{3}H scattering based on first-principles calculations is within reach.[11] For example, *ab initio* variational calculations using a hyperspherical harmonics basis expansion performed with a modern nuclear Hamiltonian consisting of an accurate nucleon–nucleon (NN) potential and a three-nucleon interaction (NNN) provide a good description of the differential cross section for elastic n + ^{3}H scattering at low energies.[12] This type of calculation is currently limited, however, to energies below the breakup threshold.

This article describes the first measurement of the differential cross section for the elastic n–^{3}H scattering at 14.1 MeV by an ICF facility. It also describes a theoretical calculation[13] of this cross section, which combines the *ab initio* no-core shell model[14] with the resonating group method[15] into a unified method (NCSM/RGM).[16] Using this theoretical approach, an accurate assessment of the n–^{3}H cross section can be made from precision data taken for the isobaric analogue p–^{3}He reaction. In these experiments, carried out on the OMEGA laser,[17] deuterium–tritium-gas–filled, thin-glass capsules were used. Each capsule, made of SiO_2, had a diameter of about 850 μm, a gas-fill pressure of about 20 atm, and a shell thickness of 3.5 μm. The fuel–gas mixture was 48.2%±0.3% deuterium, 48.8%±0.3% tritium, 2.5% hydrogen, and 0.5% helium-3 from the tritium decay. These capsules were imploded by 60 laser beams that uniformly delivered 30 kJ to the capsule in a 1-ns square pulse. Since the laser energy is quickly absorbed by the glass, the outer part of the glass shell explodes outward while the remaining part moves inward. The imploding part of the shell acts as a piston and drives a shock through the deuterium–tritium fuel that heats the ions. The glass shell continues to move inward behind the shock front, isentropically compressing the post-shock region of the fuel and additionally heating the ions to thermonuclear temperatures. Each implosion, acting as both a 14.1-MeV neutron source and a deuterium–tritium target, produced a burn-averaged ion temperature of 8.5±0.5 keV and neutron yield of about 4×10^{13}, which were measured with a neutron time-of-flight diagnostic.[18] The energy spectra of

the emitted tritons and deuterons, elastically scattered by the 14.1-MeV neutrons, were measured simultaneously using a magnet-based charged-particle spectrometer (CPS)[19] installed on the OMEGA chamber (Fig. 128.6). To cover the energy range of interest in this experiment, the detector plane of the CPS was comprised of two pieces of CR-39, which is a plastic polymer that is insensitive to γ rays and x rays produced in an implosion.[19] Different particle track characteristics in CR-39 enables the CPS to make simultaneous measurements of the scattered deuterons (d′) and tritons (t′) with energies greater than ~3.7 MeV and ~2.5 MeV, respectively (the lower-energy limits are set by the width and position of the CR-39 piece). The proton spectrum from d–d reactions was measured as well to check that the emitted charged particles were not subject to any significant energy losses in the plasma.

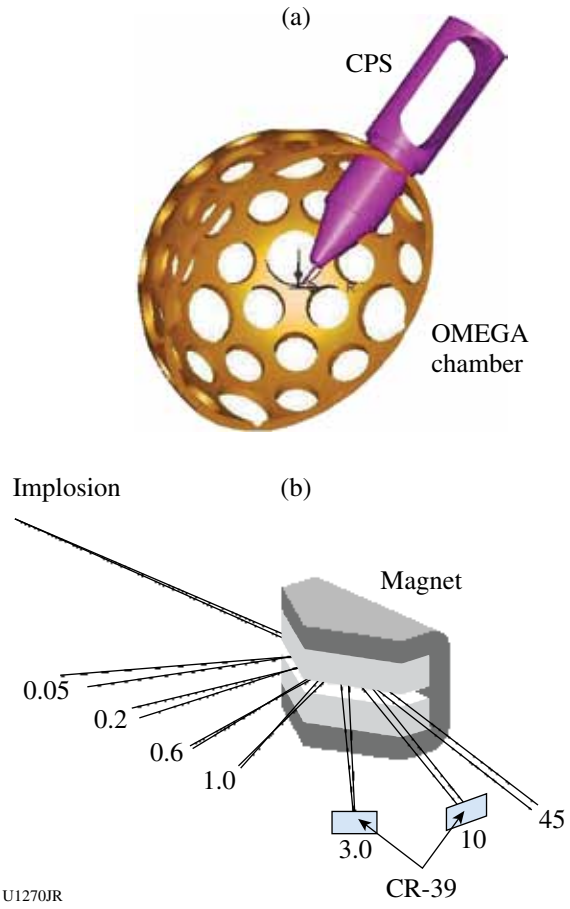

Figure 128.6
(a) The charged-particle spectrometer (CPS) on the OMEGA chamber simultaneously measures deuterons and tritons elastically scattered by 14.1-MeV neutrons and protons from d–d reactions in a deuterium–tritium-gas–filled, thin-glass capsule implosion. A bending magnet (gray) was used for momentum analysis. (b) Schematic drawing of the CPS, which uses a 2-mm-wide aperture in front of a 7.6-kG permanent magnet (Nd-Fe-B) for dispersion and high-resolution measurements of the charged particles. Two pieces of CR-39 were used to detect the dd protons and the elastically scattered deuterons and tritons. The energies are given in MeV for protons.

In Figs. 128.7(a)–128.7(c), d′ and t′ spectra measured simultaneously on three different OMEGA shots are shown. These spectra, which are background subtracted, were obtained by putting constraints on the diameter and darkness of the observed ion tracks in the CR-39 (the triton, deuteron, and background tracks have different characteristics that were used for the differentiation[19]). The remaining background that could not be rejected was characterized from regions on the CR-39, where the d′ and t′ signals cannot be detected. The error bars shown in the spectra are statistical uncertainties associated with the number of signal and background counts in each energy bin. The dd–proton spectrum measured for shot 31753 [Fig. 128.7(d)] displays an average energy that is similar to the birth energy of 3.05 MeV (temperature corrected), indicating that energy losses in the plasma are negligible. From

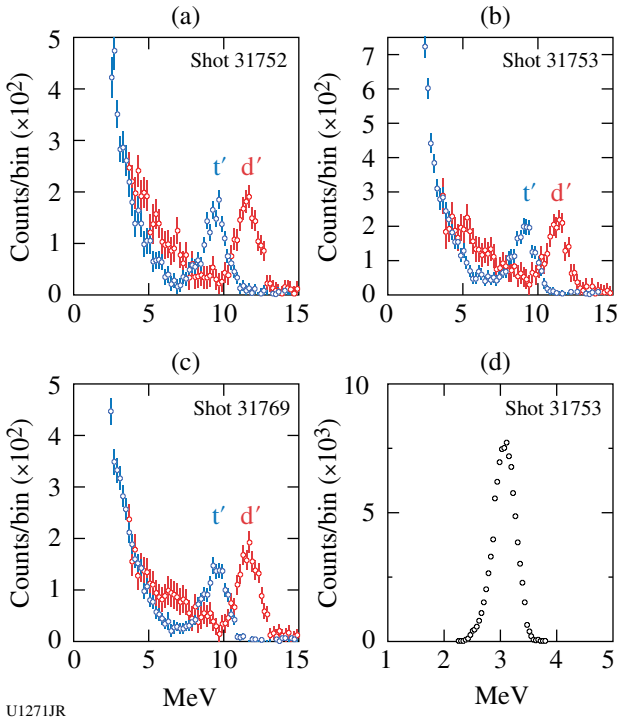

Figure 128.7
[(a)–(c)] The d′ and t′ spectra measured simultaneously on three different OMEGA shots. The broadening of these spectra is caused by the Doppler effect and CPS response. (d) The dd–proton spectrum measured for shot 31753 illustrates that the average energy is similar to the birth energy of 3.05 MeV (temperature corrected).

the measured d′ and t′ spectra, the differential cross section for the elastic n–^{3}H and n–^{2}H scattering was determined by deconvolving the CPS response[20] and the Doppler-broadened 14.1-MeV neutron spectrum.[21] While determining the n–^{2}H cross section, the effect of the deuterons from the t(n,2n)d reaction was considered and accounted for. Here, it was assumed that the cross section for this reaction was 6±4 mb, which covers the reported value in Ref. 22, or about 3%±2% of the total deuteron spectrum in the range 3.7 to 7.3 MeV. Additionally, since the plasma had a burn-averaged ion temperature of 8.5 keV, a density of ~1 g/cm^3, and a total areal density of ~2 to 3 mg/cm^2, energy-loss effects were insignificant and therefore not considered. From an energy-loss point of view, these plasma conditions correspond to a cold target with an areal density less than 0.3 mg/cm^2.

Figures 128.8(a) and 128.8(b) show the differential cross section for the elastic n–^{2}H and n–^{3}H scattering measured in this work. These cross sections, compared to the other data sets, are averages of the three measurements shown in Figs. 128.7(a)–128.7(c). The n–^{2}H cross section determined for each shot was normalized to a Faddeev calculation that is accurate to about 1%, and that normalization factor, modified by the deuterium–tritium fuel ratio, was subsequently applied to the measured n–^{3}H cross section for the same shot (the Faddeev calculation was obtained with the NNLO NN plus NNN chiral force of Ref. 23). As illustrated by Fig. 128.8(a), the angular variation of the measured n–^{2}H elastic cross section is in good agreement with the Faddeev-calculated cross section, indicating that the background subtraction, characterization of the response function, and the effect of the Doppler broadening are accurate, and that the deconvolution process provides high-fidelity data. The uncertainties shown for the n–^{3}H cross section [shown in Fig. 128.8(b) and Table 128.III] are based on the statistical uncertainty and the uncertainty associated with the normalization factor. Since the total n–^{2}H elastic cross section and the deuterium–tritium-fuel ratio in these experiments have an uncertainty of 1.0% and 0.9%, respectively, the uncertainty in the normalization factor is estimated to be 1.4%. This results in a total uncertainty ranging from 4% to 7% in the CM-angle range of 60° to 80°, which is the most important range for diagnosing ICF implosions over which the n–^{3}H cross section dominates the other ICF-relevant cross sections. This uncertainty should be contrasted to the total uncertainty larger than 20% for the Kootsey data, which is the only other data set in this angular range. Considering the uncertainties involved, the experimentally determined n–^{3}H cross section compares well with the current ENDF/B-VII evaluated cross section, which is based on Hale's *R*-matrix analysis of accurate p–^{3}He data in a wide range of energies. The fit parameters obtained in that analysis were then adjusted to account for the Coulomb effects, as explained in Ref. 9, and subsequently applied to the n–^{3}H reaction. The results from the *R*-matrix analysis are shown by the red dashed curve in Fig. 128.8(b). Another theoretical approach, described in detail in Ref. 16, was recently developed to evaluate the cross sections of light-ion reactions. This

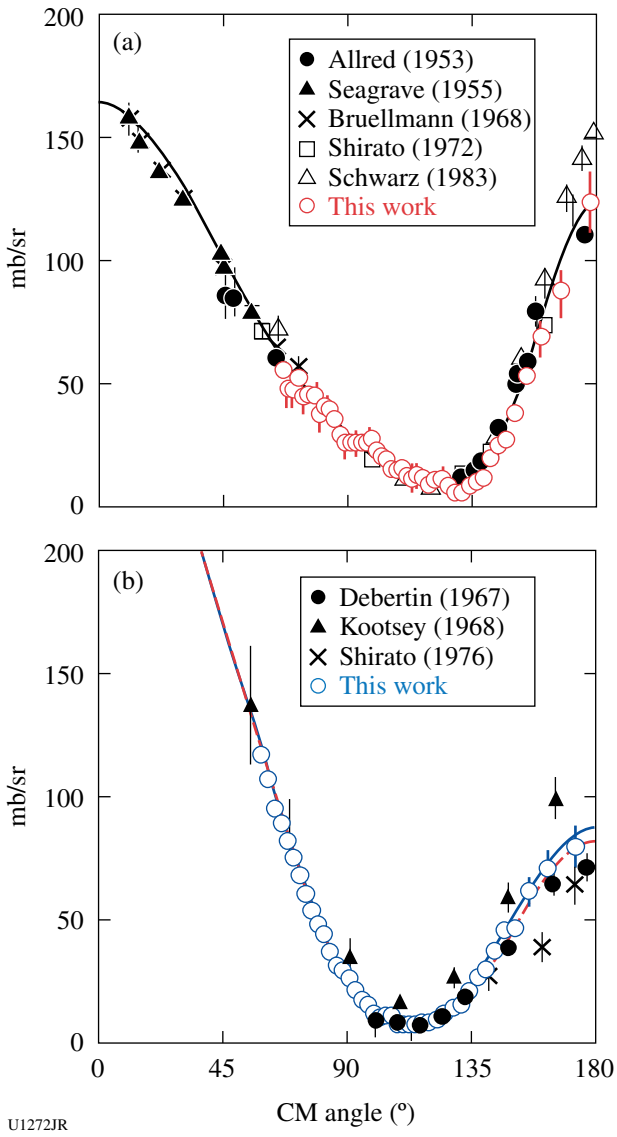

Figure 128.8
(a) Measured differential cross section for the elastic n–^{2}H scattering, which has been normalized to a Faddeev calculation. (b) Measured and calculated differential cross section for the elastic n–^{3}H scattering. The experimental data have been normalized with the deuterium–tritium fuel-ratio–modified normalization factor derived in (a). The blue solid curve represents an *ab initio* NCSM/RGM calculation; the red dashed curve represents an *R*-matrix–calculated n–^{3}H cross section

Table 128.III: Measured and calculated differential cross section for the elastic n–^{3}H scattering as a function of CM angle at 14.1 MeV. The NCSM/RGM calculation, which is corrected at forward angles as explained in the text, is considered to be accurate to about 5%.

CM angle (°)	Measured (mb/sr)	Error (mb/sr)	NCSM/RGM (mb/sr)
58.6	116.7	4.4	119.3
61.2	106.6	3.3	109.9
63.7	94.7	3.5	101.1
66.1	88.8	3.6	93.1
68.3	81.6	3.7	85.6
70.5	75.0	3.9	78.7
72.6	67.8	3.7	72.1
74.7	60.3	3.6	65.9
76.8	53.4	3.5	59.9
79.0	48.1	3.2	54.1
81.2	44.0	3.2	48.5
83.4	37.1	3.3	43.2
85.7	31.5	3.1	38.2
87.9	29.4	2.8	33.4
90.3	26.3	2.9	29.1
92.6	21.7	2.9	25.1
94.8	17.5	2.7	21.6
97.1	15.7	2.5	18.5
99.3	11.9	2.4	15.9
101.5	10.2	2.5	13.7
103.6	11.3	3.3	11.8
105.7	11.2	2.2	10.4
107.8	7.4	1.9	9.2
110.0	7.8	1.9	8.4
112.2	7.6	1.8	8.0
114.4	7.5	1.6	7.9
116.8	8.5	1.3	8.1
119.4	8.5	1.3	8.9
122.0	9.6	1.3	10.2
124.8	12.0	1.2	12.1
127.7	14.4	1.4	14.6
130.7	15.5	1.3	17.7
133.7	21.2	1.4	21.5
136.8	26.5	1.7	25.8
139.8	29.9	1.8	30.5
142.9	37.2	2.2	35.9
146.3	45.6	2.7	42.1
150.2	46.5	3.4	49.4
155.2	61.4	4.7	59.1
162.2	70.5	6.0	71.6
172.3	79.4	7.7	84.3

NCSM/RGM approach, unlike earlier *ab initio* approaches, allows one to calculate various nucleon–nucleus scattering processes for systems with A > 4, i.e., both on *s*- and *p*-shell nuclei.[13,16] The present NCSM/RGM calculations for the n–^{3}H and p–^{3}He systems use a similarity-renormalization-group–evolved chiral N^{3}LO NN interaction that includes Coulomb and other isospin breaking terms.[24] A less-than-15% inaccuracy in these calculations at forward angles is introduced by limiting the model space to channel states with the three-nucleon system in its ground state. To quantify and correct for this inaccuracy, high-precision p–^{3}He data[25] are compared to the corresponding NCSM/RGM results, and the obtained correction function is applied to the n–^{3}H calculation. The result of this procedure, which is accurate to ~5%, is illustrated by the blue solid curve in Fig. 128.8(b), which is also in good agreement with our experimental data, but differs from the *R*-matrix analysis by several percent in the backward-scattering angles of the outgoing neutron. Considering the estimated uncertainty of ~5% for the NCSM/RGM calculation, this discrepancy is, however, insignificant. Additional details of the n–^{3}H and p–^{3}He NCSM/RGM calculations are found in Ref. 13.

In summary, we report on the first measurements of the differential cross section for the elastic n–^{3}H and n–^{2}H scattering at 14.1 MeV by an ICF facility. The resulting n–^{3}H data are of higher quality than achieved in previous accelerator experiments reported in the literature and accurate enough to reliably determine the fuel ρR from the yield ratio between scattered neutrons and primary 14.1-MeV neutrons produced in an ICF implosion. The experimental results obtained at CM angles ranging from 59° to 172° are in good agreement with a theory that is based on isospin-corrected *ab initio* calculations of the isobaric analogue p + ^{3}He reaction. Both measured and calculated cross sections compare well with current ENDF/B-VII-evaluated cross section, which is based on Hale's *R*-matrix analysis. A total n–^{3}H elastic cross section of 941±47 mb was calculated using the NCSM/RGM method.

ACKNOWLEDGMENT

The authors would like to thank Prof. Dr. Evgeny Epelbaum for providing Faddeev calculations of n–^{2}H scattering at 14.1 MeV, which provided the basis for normalizing these experimental results. The work described here was supported in part by U.S. DOE (Grant No. DE-FG03-03SF22691), LLE (No. 412160-001G), LLNL (No. B504974), and General Atomics under DOE (DE-AC52-06NA27279).

REFERENCES

1. J. A. Frenje, D. T. Casey, C. K. Li, F. H. Séguin, R. D. Petrasso, V. Yu. Glebov, P. B. Radha, T. C. Sangster, D. D. Meyerhofer, S. P. Hatchett, S. W. Haan, C. J. Cerjan, O. L. Landen, K. A. Fletcher, and R. J. Leeper, Phys. Plasmas **17**, 056311 (2010).
2. B. K. Spears *et al.*, "Prediction of Ignition Implosion Performance Using Measurements of Low-Deuterium Surrogates," to be published in Physics of Plasmas.
3. G. H. Miller, E. I. Moses, and C. R. Wuest, Nucl. Fusion **44**, S228 (2004).
4. J. M. Kootsey, Nucl. Phys. **A113**, 65 (1968).
5. S. Shirato *et al.*, Nucl. Phys. **A267**, 157 (1976).
6. K. Debertin, E. Roessle, and J. U. Schott, http://www.nndc.bnl.gov/exfor/servlet/X4sGetSubent?reqx=3489&subID=21507002&plus=1, Brookhaven National Laboratory, Upton, NY (1967).
7. R. M. Devries, J. L. Perrenoud, and I. Slaus, Nucl. Phys. **A188**, 449 (1972).
8. H. S. Sherif and B. S. Podmore, in *Few Particle Problems in Nuclear Interaction*, edited by I. Slaus *et al.* (North-Holland, Amsterdam, 1972), pp. 691–694.
9. G. M. Hale *et al.*, Phys. Rev. C **42**, 438 (1990).
10. M. B. Chadwick *et al.*, Nuclear Data Sheets **107**, 2931 (2006).
11. R. Lazauskas *et al.*, Phys. Rev. C **71**, 034004 (2005).
12. M. Viviani *et al.*, Few-Body Syst. **45**, 119 (2009).
13. P. Navrátil, S. Quaglioni, and R. Roth, J. Phys., Conf. Ser. **312**, 082002 (2011); P. Navrátil *et al.*, Lawrence Livermore National Laboratory, Livermore, CA, Report LLNL-TR-423504 (2010).
14. P. Navrátil, J. P. Vary, and B. R. Barrett, Phys. Rev. Lett. **84**, 5728 (2000); P. Navrátil, J. P. Vary, and B. R. Barrett, Phys. Rev. C **62**, 054311 (2000).
15. K. Wildermuth and Y. Tang, *A Unified Theory of the Nucleus,* Clustering Phenomena in Nuclei (Vieweg, Braunschweig, Germany, 1977).
16. S. Quaglioni and P. Navrátil, Phys. Rev. Lett. **101**, 092501 (2008); S. Quaglioni and P. Navrátil, Phys. Rev. C **79**, 044606 (2009).
17. T. R. Boehly, D. L. Brown, R. S. Craxton, R. L. Keck, J. P. Knauer, J. H. Kelly, T. J. Kessler, S. A. Kumpan, S. J. Loucks, S. A. Letzring, F. J. Marshall, R. L. McCrory, S. F. B. Morse, W. Seka, J. M. Soures, and C. P. Verdon, Opt. Commun. **133**, 495 (1997).
18. V. Yu. Glebov, C. Stoeckl, T. C. Sangster, S. Roberts, G. J. Schmid, R. A. Lerche, and M. J. Moran, Rev. Sci. Instrum. **75**, 3559 (2004).

19. F. H. Séguin, J. A. Frenje, C. K. Li, D. G. Hicks, S. Kurebayashi, J. R. Rygg, B.-E. Schwartz, R. D. Petrasso, S. Roberts, J. M. Soures, D. D. Meyerhofer, T. C. Sangster, J. P. Knauer, C. Sorce, V. Yu. Glebov, C. Stoeckl, T. W. Phillips, R. J. Leeper, K. Fletcher, and S. Padalino, Rev. Sci. Instrum. **74**, 975 (2003).

20. The CPS response is described by a 300- and 1,000-keV rectangular distribution at 5 and 10 MeV, respectively. For a 8.5-keV plasma, the Doppler-broadened DT-neutron spectrum is described by a Gaussian distribution with a width of 520 keV (FWHM; see Ref. 21).

21. H. Brysk, Plasma Phys. **15**, 611 (1973).

22. I. J. Thompson, Comput. Phys. Rep. **7**, 167 (1988).

23. E. Epelbaum *et al.*, Phys. Rev. C **66**, 064001 (2002).

24. S. K. Bogner, R. J. Furnstahl, and R. J. Perry, Phys. Rev. C **75**, 061001(R) (2007); D. R. Entem and R. Machleidt, Phys. Rev. C **68**, 041001(R) (2003).

25. R. L. Hutson *et al.*, Physical Review C **4**, 17 (1971).